

CycleRL: Sim-to-Real Deep Reinforcement Learning for Robust Autonomous Bicycle Control

Gelu Liu, Teng Wang, Zhijie Wu, Junliang Wu, Songyuan Li, Xiangwei Zhu

Abstract—Autonomous bicycles offer a promising agile solution for urban mobility and last-mile logistics, however, conventional control strategies often struggle with their underactuated nonlinear dynamics, suffering from sensitivity to model mismatches and limited adaptability to real-world uncertainties. To address this, this paper presents CycleRL, the first sim-to-real deep reinforcement learning framework designed for robust autonomous bicycle control. Our approach trains an end-to-end neural control policy within the high-fidelity NVIDIA Isaac Sim environment, leveraging Proximal Policy Optimization (PPO) to circumvent the need for an explicit dynamics model. The framework features a composite reward function tailored for concurrent balance maintenance, velocity tracking, and steering control. Crucially, systematic domain randomization is employed to bridge the simulation-to-reality gap and facilitate direct transfer. In simulation, CycleRL achieves considerable performance, including a 99.90% balance success rate, a low steering tracking error of 1.15°, and a velocity tracking error of 0.18 m/s. These quantitative results, coupled with successful hardware transfer, validate DRL as an effective paradigm for autonomous bicycle control, offering superior adaptability over traditional methods. Video demonstrations are available at <https://anony6f05.github.io/CycleRL/>.

Index Terms—Deep reinforcement learning, autonomous bicycle control, sim-to-real transfer, domain randomization, under-actuated systems, lateral control.

I. INTRODUCTION

The autonomous control of two-wheeled vehicles is a classic challenge in robotics, involving stabilizing inherently unstable dynamics while executing steering maneuvers [1]. This capability is critical for emerging applications such as autonomous cycling, micro-logistics, and intelligent mobility solutions, which demand robust stability and precise lateral control in complex urban environments [2]. Consequently, autonomous bicycle control has become a key testbed for advancing control methodologies and embodied intelligence.

Two primary paradigms exist for self-balancing systems: reaction wheels and steering control. While reaction-wheel-based approaches offer static balancing capabilities [3], they

This work was supported by the National Natural Science Foundation of China under Grant No. T2350005, the Fundamental Research Funds for the Central Universities, Sun Yat-sen University under Grant No. 23xkjc008, and in part by the Young Faculty Development Program of the Fundamental Research Funds for the Central Universities under Grant No. 24qnpy206, Sun Yat-sen University, School of Electronics and Communication Engineering.

Gelu Liu, Teng Wang, Zhijie Wu, Junliang Wu, Songyuan Li, Xiangwei Zhu are with the School of Electronics and Communication Engineering and Shenzhen Key Laboratory of Navigation and Communication Integration, Sun Yat-sen University, Shenzhen 518107, China (e-mail: liuglu@mail2.sysu.edu.cn; wangt556@mail.sysu.edu.cn; wuzhj39@mail2.sysu.edu.cn; wujliang9@mail2.sysu.edu.cn; lisy287@mail.sysu.edu.cn; zhuxw666@mail.sysu.edu.cn).

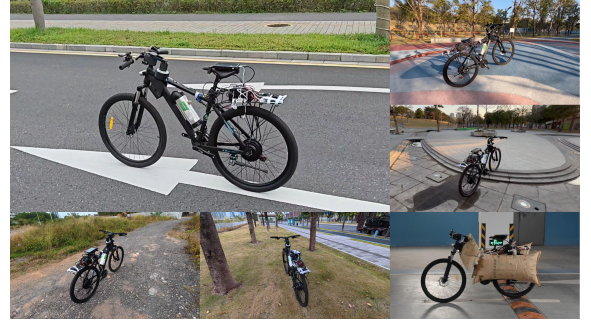


Fig. 1: Real world deployment of the proposed autonomous bicycle control framework across different conditions.

are often limited by high energy consumption, increased mechanical complexity, and payload constraints. In contrast, steering control presents a more pragmatic and efficient alternative that aligns with natural bicycle dynamics [4]. Its simplified architecture, lower energy requirements, and superior load-carrying capacity make it the preferred choice for practical, real-world applications.

Historically, steering control has been implemented via classical methods, including PID controllers [5], [6], LQR [7], MPC [8], LPV [1], and fuzzy logic [9]. However, these approaches face significant drawbacks. PID controllers demand extensive manual tuning, while model-based methods, e.g., MPC, are computationally intensive and highly sensitive to inaccuracies in system parameters. This reliance on precise models often results in controllers that are fragile to real-world variations, compromising their reliability.

These limitations have motivated the turn to Deep Reinforcement Learning (DRL), a powerful paradigm for solving complex sequential decision-making problems with high-dimensional inputs and nonlinear dynamics [10]. By leveraging high-fidelity simulators, e.g., Isaac Gym [11] and MuJoCo [12], DRL enables agents to learn optimal control strategies through autonomous interaction, thereby eliminating the need for explicit modeling. This end-to-end paradigm learns a direct mapping from sensory observations to actuator commands, which can reduce system latency and holistically optimize the control pipeline, offering superior robustness and adaptability for dynamic environments [13].

In this work, we present a DRL framework for end-to-end autonomous bicycle control. We train control policies using Proximal Policy Optimization (PPO) [14] within Isaac Sim environment, incorporating domain randomization to ensure

robust sim-to-real transfer. The resulting system is validated on a custom-built bicycle platform, demonstrating effective end-to-end control without any explicit dynamic modeling, as shown in Fig. 1. The final system achieves impressive real-world performance metrics, including a balance success rate of 99.90%, an algorithmic latency of 1 ms, and a sustained balance duration exceeding 30 minutes, highlighting the practical effectiveness of our approach.

The remainder of this paper is structured as follows: Section II reviews related work in autonomous control and DRL. Section III details our methodological framework. Section IV presents our experimental evaluations, and Section V concludes the paper. Our primary contributions are:

- A unified DRL formulation for bicycle control, featuring a composite reward function that simultaneously optimizes stability, tracking accuracy, and control smoothness, enabling end-to-end policy learning.
- A neural network architecture and training methodology that maps raw sensor data to steering commands, incorporating temporal regularization and action smoothing to ensure dynamically feasible control.
- A comprehensive sim-to-real strategy combining domain randomization to bridge the reality gap and achieve effective generalization from simulation to a physical bicycle platform.

II. RELATED WORK

A. Traditional Control Methods for Two-Wheeled Vehicles

The control of two-wheeled vehicles has been extensively addressed by traditional control methodologies. Model-based approaches such as Proportional-Integral-Derivative (PID), Linear-Quadratic Regulator (LQR), and Model Predictive Control (MPC) have been widely explored. While LQR controllers have shown to improve responsiveness and efficiency [3], [7], [15] and MPC offers superior constraint handling for trajectory tracking [8], these methods fundamentally rely on accurate system models and incur significant computational overhead.

Alternatively, knowledge-based approaches, e.g., fuzzy logic, manage system nonlinearities without requiring a precise mathematical model. Fuzzy controllers have been successfully designed to achieve robust balance and steering control under different conditions [9], [16]. However, their performance is highly dependent on extensive expert knowledge and manual tuning, which can result in suboptimal control strategies.

Despite their foundational contributions, these traditional methods generally share common limitations: high sensitivity to model inaccuracies, significant computational demand, and limited adaptability across diverse conditions. These challenges motivate the exploration of learning-based approaches that can derive robust control policies directly from interaction.

B. Learning-Based Applications in Bicycle Control

Learning-based approaches, notably imitation learning (IL) and deep reinforcement learning (DRL), have emerged as transformative paradigms in embodied control [2]. Advances in simulators, e.g., NVIDIA Isaac Gym [11] and MuJoCo [12],

have enabled massive parallel experience collection and efficient policy training, lowering the barrier for deploying neural controllers in nonlinear and underactuated systems.

IL has shown promise in bicycle motion control, primarily by leveraging expert demonstrations to achieve rapid convergence in balancing and trajectory tracking. For instance, Weissmann et al. used conditional IL for vision-based bicycle trajectory prediction, achieving good short-term accuracy [17]. However, IL policies tend to generalize poorly beyond the training distribution and often require high-quality demonstrations hard to acquire in rare scenarios, making IL less suitable for robust bicycle control in dynamic environments.

In contrast, DRL enables learning control policies through trial-and-error interactions without relying on expert data, and its capacity for complex dynamic coupling makes it highly suitable for vehicle control [18]. For instance, DRL has been employed to integrate multiple control objectives such as path tracking and stability in autonomous scooter driving scenarios [19], and to achieve robust navigation for vehicles traversing rough and varied terrains [20]. Focusing on the particularly challenging domain of two-wheeled vehicles, Guo et al. developed an RL algorithm based on the nonaffine nonlinear dynamics of a bicycle, successfully demonstrating self-balancing control with preliminary physical validation [21].

Nevertheless, achieving robust, effective sim-to-real transfer for a bicycle controlled solely through steering (i.e., without reaction wheels) remains a significant, unaddressed challenge. This difficulty stems from two primary factors: the system's inherent instability, particularly at low speeds, and its extreme sensitivity to minute physical discrepancies between the simulated and real-world models. This represents a substantial gap in advancing autonomous mobility solutions.

C. Simulation-to-Reality Transfer Technologies

A central challenge in deploying learning-based controllers is bridging the "simulation-to-reality" (sim-to-real) gap, where policies trained in simulation exhibit a significant performance degradation on physical systems [22]. This performance drop is attributable to the discrepancies between the simulated model and real-world dynamics, such as parametric inaccuracies, unmodeled stochastic dynamics, sensor noise and external disturbances.

Key strategies have been developed to bridge this gap. Domain randomization enhances policy generalization by training across a wide distribution of simulation parameters, a technique proven effective for transferring vision-based policies to real robots [23]. Other prominent methods include training ensembles of dynamics models to capture uncertainty, using adversarial training frameworks, e.g., Robust Adversarial Reinforcement Learning (RARL) to prepare for worst-case scenarios [24], and employing domain adaptation to align simulation and real-world distributions [25].

However, the application of these sim-to-real techniques to the complex dynamics of bicycle control remains largely unexplored. This presents a significant opportunity to advance the real-world deployment of autonomous two-wheeled vehicles, given their unique stability challenges and high sensitivity to environmental factors.

III. METHODOLOGY

A. Nonlinear Dynamics and Uncertainty Analysis

1) *Two-Wheeled Vehicle Dynamics*: Two-wheeled vehicles represent a canonical class of underactuated nonholonomic systems characterized by intricate coupling between rotational and translational motion that poses a significant challenge to conventional linear control synthesis.

Consider the configuration space parameterized by generalized coordinates $q = [\varphi, \delta, x, y, \psi]^T$, where φ represents the roll angle, δ denotes the steering angle, (x, y) defines the planar position, and ψ is the yaw angle, as shown in Fig. 2. The complete nonlinear dynamics can be expressed as:

$$M_\theta(q)\ddot{q} + C_\theta(q, \dot{q})\dot{q} + G_\theta(q) = B(q)u + \tau_{\text{ext}}(t) \quad (1)$$

where $M_\theta(q) \in \mathbb{R}^{5 \times 5}$ is the configuration-dependent inertia matrix, $C_\theta(q, \dot{q})$ captures velocity-dependent Coriolis and gyroscopic effects, $G_\theta(q)$ represents gravitational and centrifugal forces, $B(q)$ is the input distribution matrix, and $\tau_{\text{ext}}(t)$ denotes external disturbances [26].

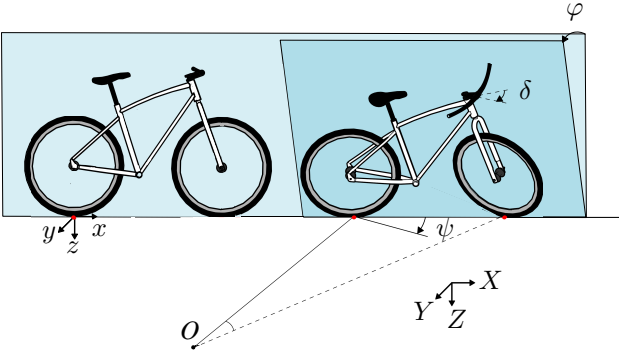


Fig. 2: Sketch of the two-wheeled vehicle [27].

2) *Stochastic Dynamics Formulation*: To rigorously account for real-world uncertainties, we characterize the system evolution using a stochastic differential equation (SDE) framework:

$$dq = f_\theta(q, u)dt + g_\theta(q)dW_t + h_\theta(q)d\xi_t \quad (2)$$

where $\theta \sim \mathcal{D}(\Theta)$ represents uncertain physical parameters (e.g., mass distribution, friction coefficients) drawn from a bounded uncertainty set. The function $f_\theta(q, u)$ denotes the *deterministic drift vector*, governing the nominal nonlinear dynamics of the bicycle. The stochastic environmental interactions are modeled by two terms: $g_\theta(q)$ is the *diffusion tensor* scaling the standard Wiener process W_t , which represents continuous disturbances such as uneven terrain vibrations; $h_\theta(q)$ represents the *jump amplitude matrix* associated with the Poisson jump process ξ_t , modeling discrete impulsive events such as collisions or sudden road steps [28].

Directly solving the optimal control problem for Eq. (2) is mathematically intractable due to the stochastic terms (W_t, ξ_t) and parametric uncertainty (θ). While traditional methods like nonlinear MPC can handle such dynamics, they typically require simplifying assumptions or computationally prohibitive online optimization. To bypass these limitations without explicit system identification, we adopt a model-free DRL approach, as detailed in the following section.

B. Reinforcement Learning Framework

1) *Markov Decision Process Formulation*: We formulate the control problem as a Markov Decision Process (MDP), defined by the tuple $\mathcal{M} = (\mathcal{S}, \mathcal{A}, \mathcal{P}, \mathcal{R}, \gamma)$. Here, $\mathcal{S} \in \mathbb{R}^n$ and $\mathcal{A} \in \mathbb{R}^m$ denote the continuous state and action spaces, respectively. \mathcal{P} governs the transition dynamics, \mathcal{R} defines the control objectives, and γ is the discount factor. Although the physical system is partially observable, we utilize the instantaneous observation vector o_t (comprising IMU and encoder data) directly as the state s_t . This approximation is justified by the high control frequency, which mitigates the need for temporal history integration. Consequently, we learn a reactive stochastic policy $\pi_\theta(a_t|s_t)$ parameterized by a standard Multi-Layer Perceptron (MLP), relying on domain randomization to ensure robustness against sensor noise.

2) *Composite Reward Function Design*: The controller's learning process is guided by a composite reward function designed to balance performance goals with control efficiency. As illustrated in Fig. 3, this function serves as a reward shaping mechanism, combining positive incentives for achieving stability and tracking objectives with negative penalties to ensure smooth and economical actions. By aggregating these components into a single scalar signal, we transform the multi-objective requirements into a tractable optimization problem.

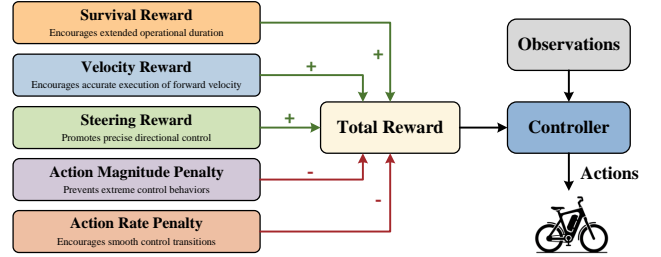


Fig. 3: Illustration of the reward function design for balancing and steering control. The total reward aggregates performance incentives (green arrows) and control effort penalties (red arrows) into a unified scalar to guide the policy learning.

The total reward R_t at each timestep is computed as the weighted sum of five key components:

$$R_t = \lambda_{\text{surv}}r_{\text{surv}} + \lambda_{\text{vel}}r_{\text{vel}} + \lambda_{\text{steer}}r_{\text{steer}} + \lambda_{\text{act}}r_{\text{act}} + \lambda_{\text{rate}}r_{\text{rate}} \quad (3)$$

where the weights are set to $\lambda_{\text{surv}} = 1.0$, $\lambda_{\text{vel}} = 3.0$, $\lambda_{\text{steer}} = 5.0$, $\lambda_{\text{act}} = 1.0$, and $\lambda_{\text{rate}} = 2.0$. These components are organized into two groups: performance-oriented rewards and control effort penalties.

a) Performance-Oriented Rewards: These components provide positive reinforcement for successfully executing the primary control tasks.

Survival Reward (r_{surv}): To encourage long-term stability, a constant positive reward is given for each timestep the bicycle remains operational. This incentivizes the agent to avoid falling.

$$r_{\text{surv}} = 1 \quad (4)$$

Velocity Tracking Reward (r_{vel}): This reward encourages the agent to accurately follow the target forward velocity (v_{cmd}). The reward is exponentially proportional to the negative error between the actual and commanded velocities.

$$r_{\text{vel}} = \exp(-\alpha|v_{\text{actual}} - v_{\text{cmd}}|) \quad (5)$$

where the error sensitivity $\alpha = 0.25$.

Steering Tracking Reward (r_{steer}): Similarly, this component rewards the agent for precise directional control by minimizing the heading error between the actual (ψ_{actual}) and desired (ψ_{desired}) heading.

$$r_{\text{steer}} = \exp(-\beta|\psi_{\text{actual}} - \psi_{\text{desired}}|) \quad (6)$$

where $\beta = 0.1$.

b) Control Effort Penalties: These components are negative rewards designed to regularize the control policy, leading to smoother and more efficient actions.

Action Magnitude Penalty (r_{act}): A penalty proportional to the L1 norm of the action (a_t) is applied to discourage aggressive policy outputs, which promotes energy efficiency.

$$r_{\text{act}} = -\|a_t\|_1 \quad (7)$$

Action Rate Penalty (r_{rate}): To ensure smooth control outputs, a penalty is imposed on the L2 norm of the change in action between consecutive timesteps. This discourages high-frequency oscillations (jerkiness).

$$r_{\text{rate}} = -\|a_t - a_{t-1}\|_2 \quad (8)$$

The hyperparameters were heuristically tuned based on a hierarchical control logic. Tracking rewards ($\lambda_{\text{vel}}, \lambda_{\text{steer}}$) are assigned significantly higher weights than the survival baseline to prevent the agent from converging to a trivial “stand-still” policy. Additionally, the steering sensitivity is set with a tighter tolerance ($\beta < \alpha$) due to the critical coupling between lateral deviations and roll instability, while penalty weights are calibrated to constrain control frequencies within the physical actuator bandwidth.

c) Episode Termination Criteria: Two distinct termination conditions are implemented to balance training efficiency with safety considerations. Timeout termination limits episodes to 64 seconds (3,200 steps at 50 Hz), while safety-based termination immediately ends episodes when $|\varphi_t| > 45^\circ$, providing clear failure signals while preventing continuation in physically unrealistic states.

3) *Proximal Policy Optimization with Composite Reward:* We employ Proximal Policy Optimization (PPO) [14] algorithm to train the control policy. Specifically, the Generalized Advantage Estimation (GAE) is directly calculated from the scalarized composite reward r_t , which guides the policy updates. The algorithm maintains the fundamental clipped surrogate objective:

$$\mathcal{L}(\theta) = \mathbb{E}_t \left[\min \left(r_t(\theta) \hat{A}_t, \text{clip}(r_t(\theta), 1 - \epsilon, 1 + \epsilon) \hat{A}_t \right) \right] \quad (9)$$

where $r_t(\theta) = \frac{\pi_\theta(a_t|s_t)}{\pi_{\theta_{\text{old}}}(a_t|s_t)}$ represents the probability ratio of the policy π_θ under current and old parameters and \hat{A}_t denotes the advantage estimate computed from the reward function.

The composite reward structure is integrated into the PPO framework via linear scalarization. Specifically, the weighted total reward R_t serves as the unified scalar signal for Generalized Advantage Estimation (GAE). By aggregating conflicting objectives into a single value, the standard PPO algorithm optimizes the policy π_θ to maximize the expected cumulative return of the composite objective.

C. Domain Randomization Strategy

As mentioned in [23], discrepancies between simulation and reality—ranging from unmodeled dynamics to unseen states—can lead to catastrophic failure on physical hardware. To bridge the reality gap and achieve robust sim-to-real generalization, we employ a decoupled hierarchical randomization strategy comprising three key components: *Dynamics Randomization*, *Initial State Randomization*, and *Task Randomization*, with parameter ranges grounded in the real-world scenarios of underactuated unstable systems (e.g., bicycles). This multi-layered strategy forces the policy to generalize across a vast set of physical conditions and operational scenarios, preventing overfitting to specific simulation artifacts.

TABLE I: Domain Randomization Variables

Randomization Variables	Range/Distribution
<i>Dynamics Randomization (Physical Parameters)</i>	
System Total Mass (m_{total})	$\mathcal{U}([15.0, 45.0])$ kg
Center of Mass Height (h_{CoM})	$\mathcal{U}([0.50, 0.80])$ m
Tire Friction Coefficient (μ)	$\mathcal{U}([0.5, 1.2])$
Actuator Force Gain	$\mathcal{U}([0.9, 1.1])$
Observation Noise	$\mathcal{N}(0, (\rho \cdot s_{\text{max}})^2)$, $\rho \sim \mathcal{U}([0.01, 0.20])$
<i>Initial State Randomization</i>	
Initial Body Velocity (v_{init})	$\mathcal{U}([1.0, 2.5])$ m/s
Initial Body Lean Angle (φ_{init})	$\mathcal{U}([-10, 10])$ deg
Initial Servo Motor Position ($\theta_{m,\text{init}}$)	$\mathcal{U}([-20, 20])$ deg
Initial Hub Motor Velocity ($\omega_{m,\text{init}}$)	$\mathcal{U}([0, 3.0])$ rad/s
<i>Task / Command Randomization</i>	
Target Velocity Command (v_{cmd})	$v_{\text{cmd}} \sim \mathcal{U}([1.0, 5.0])$ m/s, $t_{\text{resample}} \sim \mathcal{U}([3, 5])$ s
Target Steering Command (δ_{cmd})	$\delta_{\text{cmd}} \sim \mathcal{U}([-10, 10])$ deg, $t_{\text{resample}} \sim \mathcal{U}([3, 5])$ s

1) *Dynamics Randomization:* To address parametric uncertainties, modeling errors, and sensor noise, we randomize key physical and perceptual parameters of the bicycle model (see Table I). Specifically, total mass and center-of-mass height are varied to account for configuration changes and measurement inaccuracies; friction and actuator gain are randomized to capture diverse terrain conditions and hardware variations; and zero-mean Gaussian noise—scaled as a percentage of each signal’s maximum magnitude (s_{max})—is added to simulate sensor imperfections. This distributional robustness enables the policy to generalize across simulation-to-reality gaps.

2) *Initial State Randomization:* We randomize the bicycle’s initial kinematic state at the start of each episode. This simulates real-world scenarios where the controller must engage from various states of motion and tilt, forcing the agent to learn stabilization from a wide variety of unstable configurations. The resulting policy is thus significantly more resilient than one trained only from a static, upright start, ensuring safety during the critical engage-disengage transitions.

3) *Task and Command Randomization*: To develop a versatile controller, we implement task randomization by dynamically varying target velocity and steering commands within random time intervals. This compels the policy to learn a generalizable mapping from state-command pairs to actions, rather than overfitting to a static stabilization equilibrium. This capability is vital for practical deployment, enabling the agent to reliably follow high-level directives in real world.

D. System Architecture and Implementation

1) *High-Fidelity Simulation Framework*: The training environment is implemented using NVIDIA Isaac Sim, providing GPU-accelerated physics simulation with realistic sensor modeling and parallel environment execution. Isaac Sim incorporates advanced contact dynamics, variable friction and surface properties, high-fidelity IMU noise characterization, and actuator dynamics with realistic limitations. The comprehensive physical modeling also ensures that learned policies encounter the complex nonlinearities characterizing real-world vehicle-terrain interaction, as shown in Fig. 4. More details about vehicle modeling, including geometric kinematics and dynamic parameters, are available in supplementary video.

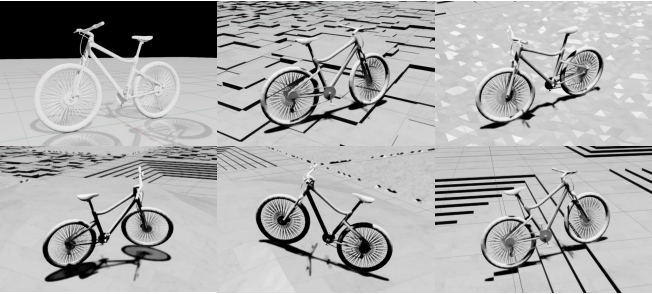


Fig. 4: Bicycle and terrain modeling in Isaac Sim.

2) *Hierarchical Control Architecture*: To support real-time onboard deployment, we established a hierarchical control architecture comprising input processing, policy inference, and actuator control layers. We employed a multi-process asynchronous framework to manage high-frequency data flow between layers, ensuring minimal end-to-end latency for the 50 Hz control loop. For detailed diagrams of the signal flow and software stack, please refer to the video.

IV. EXPERIMENTS

A. Evaluation Metrics and Implementation Details

1) *Metrics Definition on Performance*: We establish a comprehensive evaluation framework encompassing multiple performance dimensions critical for autonomous bicycle control systems. Table II summarizes the evaluation criteria across three categories.

2) *Training Configuration and Hyperparameters*: Training details, including configurations and hyperparameters, are provided in Table III. Our training infrastructure leverages NVIDIA Isaac Sim, achieving over 700,000 simulation steps per second across 16,384 parallel environments on NVIDIA RTX 4090, ensuring a considerable iteration speed.

TABLE II: Evaluation Metrics on Performance

Metric	Definition
Balance Metrics	
Balance Success Rate (BSR)	Percentage of episodes maintaining $ \varphi < 0.5$ rad.
Balance Recovery Time (BRT)	Recovery time from disturbances exceeding 0.3 rad.
Maximum Balance Duration (MBD)	Longest continuous balancing period achieved.
Critical Angle Tolerance (CAT)	Maximum recoverable roll angle maintaining BSR > 95%.
Control Metrics	
Steering Tracking Error (STE)	RMS error between commanded and actual steering.
Velocity Tracking Error (VTE)	Mean absolute error in longitudinal velocity control.
System Response Latency (SRL)	Time to reach within 10% of the target command value.
Robustness Metrics	
Maximum Noise Tolerance (MNT)	Highest sensor noise level maintaining BSR > 95%.
Minimum Sustaining Speed (MSS)	Minimum speed maintaining BSR > 95%.

TABLE III: Training Configurations

Hyperparameters	Value
PPO Hyperparameters	
Learning rate	1×10^{-4} (cosine annealing)
Discount factor γ	0.99
GAE parameter λ	0.95
Policy clip ratio ϵ	0.2
Value function coefficient	1.0
Network Architecture	
Actor network	5-layer MLP [512, 256, 128, 64] ¹
Critic network	5-layer MLP [512, 256, 128, 64] ¹
Activation function	ELU
Simulation Hyperparameters	
Parallel environments	16,384
Simulation frequency	50 Hz
Episode duration	64 seconds (3,200 steps)
Total training epochs	5,000

¹ Including 8-dim input and 2-dim output transformations.

B. Simulation Experiments and Quantitative Analysis

1) *Evaluation on Simulation Performance*: We conduct comprehensive experiments across 1,000 independent episodes to establish fundamental performance characteristics. To validate the proposed approach, we benchmark against calibrated PID and LQR baselines. PID baseline features a dual-loop structure (steer/balance) with velocity-dependent gain scaling ($K \propto v^{-2}$) to prevent high-speed oscillations and base gains were tuned to $K_p = 4.0$ and $K_d = 0.4$ via Ziegler-Nichols at 2.0 m/s. LQR baseline utilizes real-time Riccati equation solving on a linearized model to handle velocity variations, whose cost weights were set to $Q = \text{diag}[20.0, 6.0, 3.5]$ and $R = 1.5$, with steering tracking achieved by mapping δ_{cmd} to an equilibrium roll angle. Table IV presents the quantitative results across our evaluation metrics.

The results confirm the controller's superior performance compared to traditional methods. CycleRL achieves a 99.90% balance success rate, significantly outperforming the PID (30.59%) and LQR (13.27%) baselines. Notably, it demon-

TABLE IV: Comparative Simulation Performance

Metric ¹	PID	LQR	Ours
Balance Performance			
Success Rate (%) \uparrow	76.5	93.2	99.9
Recovery Time (s) \downarrow	1.41 \pm 0.22	1.47 \pm 0.21	1.05 \pm 0.18
Max. Duration (s) \uparrow	15.0	148.9	>1,800
Crit. Angle Tol. ($^\circ$) ² \uparrow	22.24	21.40	27.79
Control Performance			
Steering Error ($^\circ$) \downarrow	4.04 \pm 1.51	1.82 \pm 0.64	1.15 \pm 0.72
Velocity Error (m/s) \downarrow	\uparrow	\uparrow	0.18 \pm 0.26
Response Latency (s) \downarrow	1.67 \pm 1.12	1.27 \pm 0.61	1.06 \pm 0.17
Robustness Indicators			
Max. Noise Tol. ³ \uparrow	\uparrow	\uparrow	0.32
Min. Sustaining Spd (m/s) \downarrow	1.84	1.71	1.05

¹ Reported as Mean \pm Standard Deviation where applicable.

² Reported as the minimum of both sides (conservative estimate).

³ MNT represents the max tolerable noise amplitude fraction.

strates faster stabilization, recovering from perturbations in 1.51 s (approximately 49.16% and 29.77% faster than PID and LQR, respectively), while tolerating extreme roll angles up to 27.8 $^\circ$ (vs. 18.4 $^\circ$ for LQR). Furthermore, unlike the baselines which struggle at lower velocities, our controller maintains robust stability down to 1.05 m/s, exhibiting precise steering tracking with minimal steering error of 1.15 $^\circ$.

C. Convergence Analysis and Learning Dynamics

The policy’s training progression under 10 random seeds is depicted in Fig. 5. Stable convergence is achieved after approximately 1,000 training epochs, equivalent to 50M simulation steps. As shown in Fig. 5a, the monotonic increase and eventual plateau of both the Mean Episode Length and Mean Total Reward confirm a stable and effective learning process.

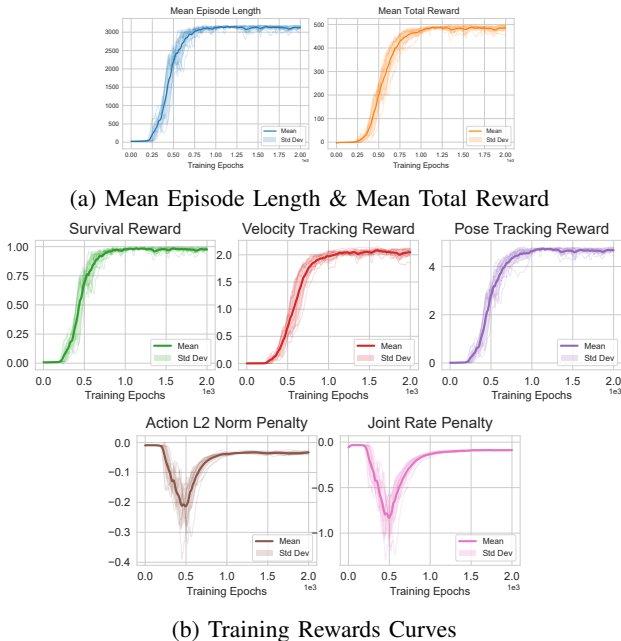


Fig. 5: Training curves and convergence analysis.

The learning dynamics, particularly the penalty curves in Fig. 5b, reveal a natural two-phase curriculum learning effect.

An initial phase of aggressive control, marked by a dip in the penalty values, allows the agent to quickly master basic stability. This is followed by a refinement phase, where the penalties decrease (rise toward zero) as the agent learns to perform the task with smoother, more efficient actions.

D. Robustness Verification Experiments

We conduct robustness evaluation across multiple challenging scenarios to assess deployment readiness. Table VI summarizes performance across diverse operational conditions.

The evaluation confirms the system’s performance and considerable resilience. Considerable performance is achieved on a smooth plane and ideal sensor configuration (99.90% BSR) and at low speeds (99.49% BSR). The system effectively handles sensor degradation, maintaining a BSR of 96.38% with severe noise and 90.84% with intermittent dropouts. On complex terrains, the system exhibits a graceful performance degradation ranging from 6.99% on rough pavement to 23.30% over gentle steps, compared to the ideal condition. Balance Recovery Time (BRT) and tracking errors (STE, VTE) also remain well-maintained across diverse conditions.

Notably, the observed BSR declines at high speeds, despite physical self-stability, can be attributed to closed-loop control limitations. Since lateral acceleration scales quadratically with velocity, the system becomes hypersensitive to steering inputs, causing over-correction. Additionally, the fixed 50 Hz control frequency may approach its bandwidth limits at high speeds, where significant state evolution between steps amplifies discretization errors and erodes the stabilization margin.

E. Ablation Studies

1) *Ablation Study of Reward Functions*: We systematically investigate individual reward component contributions through controlled ablation experiments. Table V and Fig. 6 present performance degradation when each component is removed.

TABLE V: Ablation Results of Reward Functions

Configuration	BSR (%) \uparrow	STE (deg) \downarrow	VTE (m/s) \downarrow
Complete Reward	99.90	1.15	0.18
No Survival Reward	99.99 (+0.09)	1.72 (+0.57)	0.19 (+0.01)
No Velocity Tracking	96.71 (-3.19)	1.15 (-0.00)	0.59 (+0.41)
No Steering Tracking	99.87 (-0.03)	6.30 (+5.15)	0.21 (+0.03)
No Action Penalty	99.99 (+0.09)	1.72 (+0.57)	0.38 (+0.20)
No Rate Penalty	99.87 (-0.03)	2.29 (+1.14)	0.55 (+0.37)

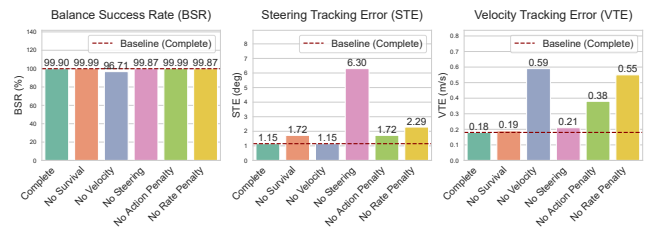


Fig. 6: Results of Reward Ablation.

The ablation analysis reveals that tracking rewards are crucial. Removing the velocity tracking reward leads to a

TABLE VI: Robustness Evaluation

Test Category	Condition	BSR (%) \uparrow	BRT (s) \downarrow	STE (deg) \downarrow	VTE (m/s) \downarrow	Notes
Velocity Range	Low speed (1.0-3.0 m/s)	99.49	1.58	1.57	0.23	Crowded conditions
	Normal speed (3.0-5.0 m/s)	86.21	2.05	1.56	0.28	Normal conditions
Sensor Degradation	No noise	99.90	1.51	1.15	0.18	Baseline performance
	Maximum noise level	96.38	2.90	3.46	0.78	20% amplitude noise
	Intermittent dropouts	90.84	1.62	1.92	0.48	10% data loss rate
Terrain Type	Flat plane	99.90	1.51	1.15	0.18	Ideal conditions
	Rough pavement	88.47	1.66	1.44	0.18	Standard road surface
	Gravel surface	85.87	2.15	1.69	0.21	Reduced traction
	Slope terrain	92.05	1.74	1.35	0.23	Slope adaptation
	Gentle steps	76.60	1.80	1.31	0.22	Complex terrain

significant stability performance drop (BSR -3.19%, VTE +0.41 m/s); the steering tracking reward follows a similar pattern. Interestingly, removing the survival reward and action penalty slightly improves the BSR, suggesting a potential conservative bias. Finally, the absence of the rate penalty harms control smoothness, increasing both STE and VTE.

2) *Impact Assessment of Domain Randomization*: Table VII evaluates the contribution of different randomization strategies to sim-to-real transfer effectiveness.

TABLE VII: Component Analysis of Domain Randomization

Randomization Strategy	BSR (%) \uparrow	STE (deg) \downarrow	VTE (m/s) \downarrow
Full Randomization	99.90	1.15	0.18
No Randomization	99.99 (+0.09)	5.16 (+4.01)	0.49 (+0.31)
Dynamics-Only	99.95 (+0.05)	2.49 (+1.34)	0.43 (+0.25)
Initial States-Only	99.99 (+0.09)	4.03 (+2.88)	0.57 (+0.39)
Command-Only	99.19 (-0.71)	1.72 (+0.57)	0.20 (+0.02)
Terrain-Only	99.99 (+0.09)	3.84 (+2.69)	0.58 (+0.40)

The analysis reveals the significant impact of different randomization strategies. The Full Randomization strategy achieves the best overall performance with the lowest tracking errors (STE 1.15 deg, VTE 0.18 m/s). Conversely, training with No Randomization severely degrades precision, sharply increasing STE and VTE. Single-component randomizations, e.g., Dynamics-Only, Initial States-Only or Terrain-Only, also result in substantial performance loss, particularly in velocity control. These results confirm that a comprehensive, full randomization is essential for robust sim-to-real transfer.

F. Implementation and Validation of Hardware System

1) *Construction of Physical Platform*: Our hardware validation utilizes a custom-designed bicycle platform, tailored for real-world evaluation, as shown in Fig. 7. Specifications of this hardware are detailed in Table VIII.

The mechanical design emphasizes modularity and reliability, with precision-machined interfaces minimizing mechanical compliance. The computational architecture provides sufficient processing power for real-time neural network inference while maintaining power efficiency for extended operation.

2) *Validation of Real-World Deployment*: Real-world validation was conducted to evaluate the policy’s performance, systematically comparing simulation predictions to hardware measurements as shown in Table IX.

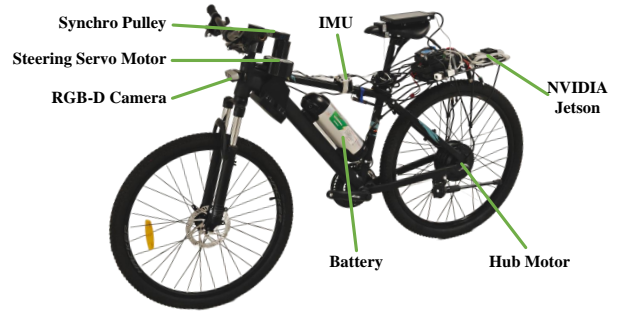


Fig. 7: Construction of hardware platform.

TABLE VIII: Specifications of Hardware Platform

Component	Specification
<i>Mechanical Platform</i>	
Wheelbase	1,100 mm
Total mass	25.0 kg (including electronics)
Center of gravity height	0.65 m
<i>Computational System</i>	
Main processor	Jetson Orin NX 16GB
Operating system	Ubuntu 20.04
<i>Sensing and Actuation</i>	
IMU	WheelTec N100
Steering servo motor	Unitree GO-M8010-6
Hub motor	BaFang RM G020.500.D
Power system	48V 9.6Ah lithium battery

To validate the policy’s efficacy as a robust controller, we employed two command modalities. In the *human-in-the-loop* configuration, high-level directives (v_{cmd} , δ_{cmd}) were provided by a remote operator, with the CycleRL policy autonomously managing the actuation for stability. To further demonstrate higher-level autonomy, we integrated a *vision-based lane tracking system* that automatically generates steering references. The policy was tested across diverse conditions, including flat surfaces, gravel paths, rugged grass, ramps, varying payloads and velocities, tire anomalies and lateral perturbations. Videos can be available at [video link](#).

The results confirm a direct sim-to-real transfer, achieving transfer ratios between 0.56 and 1.00 across key metrics, where a value of 1.00 indicates perfect transference. The most notable degradation, Steering Tracking Error (ratio: 0.56), is attributed to unmodeled IMU noise. Conversely, Velocity Tracking Error was nearly eliminated (ratio: 1.00), as the velocity command

TABLE IX: Comparison of Sim and Real Performance

Metric	Sim	Real	Transfer Ratio \uparrow
Balance Success Rate (%)	99.90	95.00	0.95
Balance Recovery Time (s)	1.05	1.29	0.81
Maximum Balance Duration (s)	>1,800	>1,800	1.00
Critical Angle Tolerance (deg)	27.79	20.12	0.72
Steering Tracking Error (deg)	1.15	2.04	0.56
Velocity Tracking Error (m/s)	0.18	0.01	1.00
System Response Latency (s)	1.06	1.10	0.96
Minimum Sustaining Speed (m/s)	1.05	1.33	0.79

was directly mapped to motor speed, bypassing wheel slip. These results validate the policy’s real-world effectiveness.

Notably, real-world comparisons with the baselines are omitted, as they failed to directly stabilize the physical platform due to severe sensitivity to model mismatches. This stark contrast underscores that our DRL approach, combined with domain randomization, effectively bridges the Sim-to-Real gap that rendered traditional methods inoperable.

V. CONCLUSION

This work presented a deep reinforcement learning framework for the robust lateral control of an autonomous bicycle. By training an end-to-end policy, our model-free approach successfully navigates the vehicle’s complex, underactuated dynamics, outperforming traditional model-based controllers while bypassing the need for explicit system identification.

Our key contributions include a composite reward function that balances stability with tracking objectives, and a comprehensive domain randomization strategy, which proved crucial for bridging the reality gap, enabling successful transfer of the learned policy. Extensive real-world experiments validated the controller’s robustness across diverse conditions, confirming its viability for autonomous cycling applications.

Future work will focus on extending this framework to include vision-based navigation and multi-agent coordination. The success of our approach demonstrates the potential of model-free DRL for developing robust and intelligent mobility systems, contributing to sustainable urban transportation.

REFERENCES

- [1] T.-J. Yeh, T.-C. Lin, and A. C.-B. Chen, “Robust balancing and trajectory control of a self-driving bicycle,” *IEEE Transactions on Control Systems Technology*, vol. 32, no. 6, pp. 2410–2417, 2024.
- [2] S. Kuutti, R. Bowden, Y. Jin, P. Barber, and S. Fallah, “A survey of deep learning applications to autonomous vehicle control,” *IEEE Transactions on Intelligent Transportation Systems*, vol. 22, no. 2, pp. 712–733, 2020.
- [3] W.-H. Huang, P. T.-T. Nguyen, D.-D. Nguyen, H.-P. Doan, M.-Y. Chuang, and C.-H. Kuo, “Stability control and path tracking of a self-balancing bicycle with a reaction wheel,” *IEEE/ASME Transactions on Mechatronics*, 2025.
- [4] W. Deng, S. Moore, J. Bush, M. Mabey, and W. Zhang, “Towards automated bicycles: Achieving self-balance using steering control,” in *Dynamic Systems and Control Conference*, vol. 51906. American Society of Mechanical Engineers, 2018, p. V002T24A012.
- [5] Y. Yu and M. Zhao, “Steering control for autonomously balancing bicycle at low speed,” in *2018 IEEE International Conference on Robotics and Biomimetics (ROBIO)*. IEEE, 2018, pp. 33–38.
- [6] J. Pei, L. Deng, S. Song, M. Zhao, Y. Zhang, S. Wu, G. Wang, Z. Zou, Z. Wu, W. He *et al.*, “Towards artificial general intelligence with hybrid tianjic chip architecture,” *Nature*, vol. 572, no. 7767, pp. 106–111, 2019.
- [7] T. Li, X. Wang, J. Li, and H. Mao, “A variable gain lqr control for a front drive motor bicycle model,” in *2025 8th International Conference on Advanced Algorithms and Control Engineering (ICAACE)*. IEEE, 2025, pp. 796–801.
- [8] G. Bellegarda and Q. Nguyen, “Dynamic vehicle drifting with nonlinear mpc and a fused kinematic-dynamic bicycle model,” *IEEE Control Systems Letters*, vol. 6, pp. 1958–1963, 2021.
- [9] A. Shafiekhani, M. J. Mahjoob, and M. Akraminia, “Design and implementation of an adaptive critic-based neuro-fuzzy controller on an unmanned bicycle,” *Mechatronics*, vol. 28, pp. 115–123, 2015.
- [10] A. Folkers, M. Rick, and C. Büskens, “Controlling an autonomous vehicle with deep reinforcement learning,” in *2019 IEEE Intelligent Vehicles Symposium (IV)*. IEEE, 2019, pp. 2025–2031.
- [11] V. M. *et al.*, “Isaac gym: High performance gpu based physics simulation for robot learning,” in *Proceedings of the Neural Information Processing Systems Track on Datasets and Benchmarks*, J. Vanschoren and S. Yeung, Eds., vol. 1, 2021.
- [12] E. Todorov, T. Erez, and Y. Tassa, “Mujoco: A physics engine for model-based control,” in *2012 IEEE/RSJ International Conference on Intelligent Robots and Systems*. IEEE, 2012, pp. 5026–5033.
- [13] D. Li, D. Zhao, Q. Zhang, and Y. Chen, “Reinforcement learning and deep learning based lateral control for autonomous driving,” *IEEE Computational Intelligence Magazine*, vol. 14, no. 2, pp. 83–98, 2019.
- [14] J. Schulman, F. Wolski, P. Dhariwal, A. Radford, and O. Klimov, “Proximal policy optimization algorithms,” *arXiv:1707.06347*, 2017.
- [15] C.-F. Huang, Y.-C. Tung, and T.-J. Yeh, “Balancing control of a robot bicycle with uncertain center of gravity,” in *2017 IEEE International Conference on Robotics and Automation (ICRA)*. IEEE, 2017, pp. 5858–5863.
- [16] C.-L. Hwang, H.-M. Wu, and C.-L. Shih, “Fuzzy sliding-mode underactuated control for autonomous dynamic balance of an electrical bicycle,” *IEEE Transactions on Control Systems Technology*, vol. 17, no. 3, pp. 658–670, 2009.
- [17] A. Weißmann and D. Görge, “An empirical study on ego vehicle trajectory prediction for bicycles in urban environments based on conditional imitation learning,” in *2021 IEEE International Intelligent Transportation Systems Conference*. IEEE, 2021, pp. 1482–1489.
- [18] H. Liu, B. Kiumarsi, Y. Kartal, A. Taha Koru, H. Modares, and F. L. Lewis, “Reinforcement learning applications in unmanned vehicle control: A comprehensive overview,” *Unmanned Systems*, vol. 11, no. 01, pp. 17–26, 2023.
- [19] J. Baltes, G. Christmann, and S. Saeedvand, “A deep reinforcement learning algorithm to control a two-wheeled scooter with a humanoid robot,” *Engineering Applications of Artificial Intelligence*, vol. 126, p. 106941, 2023.
- [20] V. Wiberg, E. Wallin, T. Nordfjell, and M. Servin, “Control of rough terrain vehicles using deep reinforcement learning,” *IEEE Robotics and Automation Letters*, vol. 7, no. 1, pp. 390–397, 2022.
- [21] L. Guo, H. Lin, J. Jiang, Y. Song, and D. Gan, “Combined control algorithm based on synchronous reinforcement learning for a self-balancing bicycle robot,” *ISA Transactions*, vol. 145, pp. 479–492, 2024.
- [22] S. Höfer, K. Bekris, A. Handa, J. C. Gamboa, M. Mozifian, F. Golemo, C. Atkeson, D. Fox, K. Goldberg, J. Leonard *et al.*, “Sim2real in robotics and automation: Applications and challenges,” *IEEE Transactions on Automation Science and Engineering*, vol. 18, no. 2, pp. 398–400, 2021.
- [23] J. Tobin, R. Fong, A. Ray, J. Schneider, W. Zaremba, and P. Abbeel, “Domain randomization for transferring deep neural networks from simulation to the real world,” in *2017 IEEE/RSJ International Conference on Intelligent Robots and Systems (IROS)*. IEEE, 2017, pp. 23–30.
- [24] P. Zhai, X. Wei, T. Hou, X. Ji, Z. Dong, J. Yi, and L. Zhang, “Robust proximal adversarial reinforcement learning under model mismatch,” *IEEE Robotics and Automation Letters*, vol. 9, no. 11, pp. 10248–10255, 2024.
- [25] J. Truong, S. Chernova, and D. Batra, “Bi-directional domain adaptation for sim2real transfer of embodied navigation agents,” *IEEE Robotics and Automation Letters*, vol. 6, no. 2, pp. 2634–2641, 2021.
- [26] R. S. Sharp, “Stability, control and steering responses of motorcycles,” *Vehicle System Dynamics*, vol. 35, no. 4-5, pp. 291–318, 2001.
- [27] N. Persson, M. C. Ekström, M. Ekström, and A. V. Papadopoulos, “Trajectory tracking and stabilisation of a riderless bicycle,” in *2021 IEEE International Intelligent Transportation Systems Conference (ITSC)*. IEEE, 2021, pp. 1859–1866.
- [28] S. Yasuda, T. Kumagai, and H. Yoshida, “Safe and efficient dynamic window approach for differential mobile robots with stochastic dynamics using deterministic sampling,” *IEEE Robotics and Automation Letters*, vol. 8, no. 5, pp. 2614–2621, 2023.